

Hydrodynamic approximations for driven dense colloidal mixtures in narrow poresFrantišek Slanina¹* and Miroslav Kotrla¹*Institute of Physics, Academy of Sciences of the Czech Republic, Na Slovance 2, CZ-18221 Praha, Czech Republic*

(Received 22 December 2022; accepted 9 June 2023; published 21 June 2023)

The system of driven dense colloid mixtures is studied in one-, two-, and three-dimensional geometries. We calculate the diffusion coefficients and mobilities for each particle type, including cross-terms, in a hydrodynamic limit, using a mean-field-type approximation. The set of nonlinear diffusion equations are then solved. In one dimension, analytical results are possible. We show that in mixtures, the “Brazil nut” phenomenon, or depletion of larger particles by force of smaller ones, appears quite generically. We calculate the ratchet current and quantify the capability of sorting particles according to their size. We also indicate that the “Brazil nut” effect lies behind the possibility of perfect separation, where large and big particles travel in strictly opposite direction.

DOI: [10.1103/PhysRevE.107.064606](https://doi.org/10.1103/PhysRevE.107.064606)**I. INTRODUCTION**

Suspensions of colloid particles flowing through constrained environments find numerous technological applications [1–5]. One of the basic tasks in this important area is sorting the mixture of colloid particles according to their size, shape, chirality, and other properties. Among the prominent sorting strategies let us mention the purely hydrodynamic Segre-Silberberg effect [3,6], the dynamic lateral displacement method [7], or the ratchet mechanism [8–15]. In this work we focus on the latter method. It is based on the flow of colloidal suspension through a pore (or rather huge ensemble of pores pierced through a membrane) under the influence of periodic external unbiased driving [1,16]. The rectification of the ratchet current is due to asymmetric geometry of the pore. Depending on the particle size, pore diameter, and frequency of the driving, the dynamics of the particles can be dominated by Brownian motion [8,11], by hydrodynamics [13], or by a combination of both [14,15].

Such systems are fairly well understood on one-particle level, thus describing low-density colloidal suspensions. However, dense colloid mixtures pose serious problems, and many of them remain only partially resolved [17–19]. Here the area touches on one side the mechanics of granular (or in general particulate) matter [20], on another side the geometry of sphere packings [21–23], and on yet another side the stochastic dynamics of exclusion processes [24,25].

In this work, we consider particles moving along a tube which is not plain and straight but is shaped and structured in various ways. The particles can be grains of sand of size around one millimeter falling down by gravity or electrostatically charged colloid particles of micrometer size driven by external electric field or blood cells flowing in a vein or something analogous. The particles scatter and interact among each other. They may move freely or get jammed. They may concentrate in certain places and leave other places

nearly void. Here we aim at describing such a complex swirl in a schematic and highly simplified way. The buildup of a schematic description proceeds in several steps. In the first step we replace the Newtonian mechanics of the particles accompanied by energy dissipation and interaction with surrounding fluid (be it air or water or oil or anything else) by purely stochastic process. We also replace the irregular shapes of the particles by perfect spheres. Elastoplastic properties of the particles as well as fluid-mediated hydrodynamic interactions between them are replaced by simple requirement that the centers of the spheres may not come closer than the sum of their radii. In the second step we discretize the Euclidean space, dividing it into cells of finite size. Specific position of particles within a single cell is neglected and we retain just information on which cell contains which particle. Particles hop between cells stochastically. In the third step we take a look at the system from a distance. We cannot distinguish each single cell any more but they look like a continuum. In this view the dynamics becomes deterministic again and is described by (nonlinear) partial differential equations. All nontrivial features of the particles we started with, i.e., their size, weight, mobility, etc., are embodied in the nonlinearities of these equations. The only task which remains now is to solve the equations, either numerically or, in a lucky case, analytically. The aim of this work is to provide a host of such solutions.

We shall suppose that the movement of the colloid particles is purely stochastic, reducing the hydrodynamic effects to bare homogeneous external drift or constant bias in hopping rates. This is a radical trivialization of the problem, as the hydrodynamics of the fluid medium surrounding all the particles not only provides a driving force, but also substantially changes the inter-particle interactions, providing a long-range and fundamentally nonadditive contribution to particle-particle and particle-wall interaction. Treating these effects is a separate and difficult task, therefore we shall skip it completely in this work.

Therefore, we base our models on the ground of stochastic exclusion processes. The prominent representative of

*slanina@fzu.cz

this set of models is the asymmetric simple exclusion process (ASEP), which was solved exactly by several methods [26–35]. The most stunning feature of this model is the absence of spatial correlations in stationary state. It was shown that this feature is moderately robust, in the sense that various generalizations of ASEP suggested in the literature [36–42] on one side do exhibit spatial correlations, but on the other side these correlations are short-ranged and in a few special cases can be calculated exactly by a cluster mean-field approximation [36,37,41]. In these cases the correlations decay with a strictly exponential tail.

In a recent series of papers [43–45] we suggested another generalization of ASEP, following earlier works of Refs. [46–52], where the generalized symmetric exclusion process was investigated. The core of the generalization consists in allowing not just one particle on a lattice point, but a number not exceeding a fixed limit k . Moreover, we allowed several species of particles characterized by different sizes. In this case the exclusion constraint means that the sum of sizes of all particles on a single site cannot exceed the limit k . Most importantly, we found that in such generalized ASEP model the long-range correlations in stationary state decay algebraically, with an exponent whose value is conjectured to be exactly 2. Despite the long-range correlations, the mean-field and cluster mean-field approximations were found to be reasonably reliable in calculation of nearest-neighbor correlations as well as particle currents. Indeed, currents depend explicitly only on short-range correlations and the nontrivial long-range correlations enter just indirectly.

This fact encourages us to perform a continuous approximation of the generalized ASEP model. The coarse-graining procedure with proper scaling limit leads to hydrodynamic equations in which only long-wavelength modes associated with locally conserved quantities survive, while all the fast-decaying short-wavelength modes are projected out [53]. To establish the validity of the hydrodynamic limit is a difficult task, but there are cases where it is resolved with mathematical rigor [46,47,53]. There are various sources of difficulties. For example, the long-range stationary correlations may easily spoil the scaling limit. We found that such correlations are indeed present in the generalized ASEP model studied here [45]. Fortunately, for the one-component variant of our generalized ASEP, with slightly different hopping rates, the existence of hydrodynamic limit was proved [47], which encourages us to assume that the hydrodynamic limit is well defined also in our case, and especially for systems with several types of particles.

Hydrodynamic equations are just expressions of conservation laws. For each conserved quantity the temporal change of its local density equates to the divergence of the associated current. The form of the equations may differ depending on the number and type (scalar, vector, etc.) of the conserved quantities. In this article it will be the set of a few scalars, namely the densities of particles of several types. The currents are themselves functionals of all the densities. These are the constitutive relations characteristic of the model in question. In the simplest case such functional is local and depends on derivatives of the densities up to a finite order.

At this point we must stress that the coarse-graining and continuum limit can be performed in (at least) two different

scaling regimes [48]. In the Eulerian scaling, time is scaled linearly with space, while in diffusion scaling time scales with square of space. In diffusion scaling we assume that in the current functional the first spatial derivative is connected to the diffusion coefficient, while higher derivatives are irrelevant in renormalization-group sense. However, in Eulerian scaling we assume that already the first spatial derivative is irrelevant and the dynamics is ballistic. To study the fluctuations, diffusion term is added phenomenologically, together with Gaussian noise, whose properties are related to the diffusion coefficient via fluctuation-dissipation theorem. This way we arrive at fluctuating hydrodynamics [54–60]. Alternative route is taken in the macroscopic fluctuation theory [61,62] which is based on assumption that not only the microscopic dynamics of the system, but also its adjoint dynamics possess well-defined hydrodynamic limit. (This is trivially satisfied for reversible dynamics, as it is self-adjoint.)

In our work we shall follow the path of diffusion scaling. Then, the basic step in solving the model in question is to establish the density dependence of the transport coefficients. Let us stress once more, that in principle the long-range correlations may lead to nonvanishing higher spatial derivatives or nonlocality, but we proceed assuming these effects irrelevant.

Calculation of diffusion and mobility coefficients is simplified in models with gradient property [53]. For nongradient systems with reversible dynamics, variational procedure is in principle exact [53] but computationally demanding [52,63]. Unfortunately, the models investigated in this work are not gradient and not reversible, so we have to resort to approximations. In a low-density limit it is possible to use perturbative approach [64], but here we need a solution for entire range of allowed densities. Mean-field-type approximations often lead to results which deviate very little from exact numbers [50,51,65,66]. However, we should be careful in interpreting the results. For example, when investigating subtle effects, like Casimir forces [67–69], such tiny deviations translate in substantial differences [66,70]. However, the argument based on variational principle [53] suggests that the mean-field-type approximations give weak but exact upper bound on the true diffusion coefficient [52,63].

The aim of our work is calculation of transport coefficients for generalized ASEP model with several types of particles differentiated by their size and with cell capacity k , $1 < k < \infty$. The calculation relies on a mean-field-type approximation, neglecting spatial correlations in a nonequilibrium state. We then apply the obtained formulas to specific examples of driven colloid mixtures in quasi one-dimensional narrow pores. When mapped on piecewise one-dimensional geometries, it is possible to obtain analytical results. One of the specific questions investigated will be the possibility of perfect separation of particles according to their size.

II. FROM CONTINUOUS TO DISCRETE MODEL AND BACK

A. Local mixing approximation

In our previous work [45] we studied the system of dense colloid mixture using an approach we called local mixing approximation. It consists in emulating the stochastic motion

of hard spherical particles by a discrete generalized ASEP. Let us briefly recall the idea here. For more details, we refer the reader to Ref. [45]. For simplicity, the formulas written in this subsection will describe movement in one dimension only, but we shall consider general dimension in the following.

We consider the system of spherical colloid particles interacting by steric repulsion. The particles may be of different sizes, the diameter of i th particle being d_i . In absence of other particles, each particle taken individually would perform a Brownian motion with bias. For the coordinate x_i of the center of i th particle we have a standard stochastic equation

$$dx_i(t) = f_i dt + dW_i(t), \tag{1}$$

where $W_i(t)$ is an ensemble of independent Wiener processes, $(dW_i)^2 = 2D_i dt$. The diffusion coefficient D_i and the drift f_i depend only on the diameter of the particle (they are both inversely proportional to d_i). In the following we shall classify the particles into M types according to their diameter. Then, the transport coefficients will be denoted $D_{0\alpha}$ and $f_{0\alpha}$ for all particles which belong to type α . The “0” in the index indicates, that the diffusion coefficient and drift pertain to noninteracting Brownian motion.

The hard-sphere interaction between particles is expressed by the constraint

$$|x_i(t) - x_j(t)| > \frac{1}{2}(d_i + d_j), \tag{2}$$

which must be valid at all times. The trajectories produced by the process (1) but violating Eq. (2) are forbidden. This constraint makes the dynamics nontrivial. We may describe it formally as follows. Let us suppose we find the probability measure $\mu_0[\{x_i(t)\}_{i=0}^N]$ in the space of all possible trajectories $x_i(t)$, $i = 1, \dots, N$, $t \in [t_0, t_1]$ of the ensemble if N particles, which started at time t_0 and ended at time t_1 . The measure μ_0 is generated by the stochastic process (1). Then, in this space of trajectories we define the indicator function $\chi[\{x_i(t)\}_{i=0}^N]$ such that $\chi = 1$ if Eq. (2) is satisfied for all i, j and all $t \in [t_0, t_1]$. Otherwise, $\chi = 0$. Then the proper measure of our process in the space of all trajectories is

$$\mu[\{x_i(t)\}_{i=0}^N] = \frac{1}{\Xi} \mu_0[\{x_i(t)\}_{i=0}^N] \chi[\{x_i(t)\}_{i=0}^N], \tag{3}$$

where the number Ξ ensures the proper normalization.

We performed practical computer simulation of this process in our previous work [45]. Interested readers may find the details on the numerical implementation there.

To simplify the situation, we emulate the continuous process (1) by a discrete one. To this end, we partition the space into disjoint cells and neglect the dynamics of the particles within the cells. The particles can hop from one cell to the next one with rates depending on the particle type. The position of the i th particle evolves according to

$$x_i(t) - x_i(0) = S_+(t) - S_-(t), \tag{4}$$

where $S_+(t)$ and $S_-(t)$ are Poisson processes with rates a_α and b_α , respectively. The rates depend only in the type α of the particle i . They are related to the properties of the process (1) as $a_\alpha - b_\alpha = f_{0\alpha}$, $a_\alpha + b_\alpha = 2D_{0\alpha}$. For simplicity, we fix the unit length as the cell size.

The constraint (2) is taken into account by the requirement that only certain configurations of particles can enter into the

cell. More specifically, we fix a cell capacity k and weight factors c_α which are related to particle diameters. If there are n_α particles of type α inside a cell, then we require that the cell capacity is not exceeded, i.e.,

$$\sum_{\alpha=1}^M c_\alpha n_\alpha \leq k. \tag{5}$$

This constraint must be satisfied at all cells and all times. Trajectories produced by the process (4) but violating the constraint (5) are forbidden.

Such an approximation effectively assumes that the dynamics within cell is fast, so that the particles are mixed on the level of cells and for description of the global behavior of the mixture it is sufficient to consider inter-cell hopping constrained by the condition (5). Hence, the name local mixing approximation.

In our previous work [45] we compared the simulation results coming from the continuous stochastic process (1), (2) with those of the discrete process (4), (5). This comparison indicates how the parameters k and c_α should be chosen to get optimal match of the continuous and discrete processes.

B. Hydrodynamic approximation

Hydrodynamic approximation assumes that relative changes of particle concentrations are small on the scale of lattice constant. It is a nontrivial problem of mathematical physics, whether a well-defined hydrodynamic limit exists [53]. Intuitively, we expect that dynamics of slow modes related to conserved quantities (in our case densities of particles of each type) give rise to hydrodynamic equations of diffusion type, while all other fast modes are effectively averaged out. There is quite important set of models in which the existence of hydrodynamic limit is proved rigorously [53]. However, here we remain on rather heuristic level. The task is to calculate density dependence of transport coefficients, i.e., the diffusion coefficients and drifts. In our derivation we rely on Refs. [50,51,65,66], but we generalize these results for the case of multicomponent system. More detailed derivation of our formulas using an alternative method will be published elsewhere [71].

In the following we suppose there are just two types of particles, called “small” and “big,” with size factors $c_s = 1$, $c_b = 2$. Therefore, the number of n_s of small and n_b of big particles in a single cell must satisfy the constraint $n_s + 2n_b \leq k$. The key quantities in the derivation of transport coefficients are the probabilities

$$\begin{aligned} \bar{P}_s &= \text{Prob}\{n_s + 2n_b = k\}, \\ \bar{P}_b &= \text{Prob}\{n_s + 2n_b \geq k - 1\} \end{aligned} \tag{6}$$

of such configurations that do not accommodate any extra small and big particle, respectively. In a homogeneous stationary state these probabilities are functions of average densities ρ_s and ρ_b of small and big particles. In hydrodynamic limit, densities are (slowly changing) functions of coordinate, and so are also $\bar{P}_s(\rho_s, \rho_b)$ and $\bar{P}_b(\rho_s, \rho_b)$. The two-component

diffusion problem is governed by equations

$$\begin{aligned} \frac{\partial}{\partial t} \rho_s &= \nabla \cdot [D_{SS}(\rho_s, \rho_b) \nabla \rho_s + D_{SB}(\rho_s, \rho_b) \nabla \rho_b - \mathbf{f}_s(\rho_s, \rho_b) \rho_s], \\ \frac{\partial}{\partial t} \rho_b &= \nabla \cdot [D_{BS}(\rho_s, \rho_b) \nabla \rho_s + D_{BB}(\rho_s, \rho_b) \nabla \rho_b - \mathbf{f}_b(\rho_s, \rho_b) \rho_b], \end{aligned} \quad (7)$$

and the transport coefficients can be expressed, using methods of Refs. [50,51], as

$$\begin{aligned} \mathbf{f}_s &= \mathbf{f}_{0s}[1 - \bar{P}_s(\rho_s, \rho_b)] \\ \mathbf{f}_b &= \mathbf{f}_{0b}[1 - \bar{P}_b(\rho_s, \rho_b)] \\ D_{SS} &= D_{0s} \left[1 - \bar{P}_s(\rho_s, \rho_b) + \rho_s \frac{\partial}{\partial \rho_s} \bar{P}_s(\rho_s, \rho_b) \right] \\ D_{SB} &= D_{0s} \rho_s \frac{\partial}{\partial \rho_b} \bar{P}_s(\rho_s, \rho_b) \\ D_{BS} &= D_{0b} \rho_b \frac{\partial}{\partial \rho_s} \bar{P}_b(\rho_s, \rho_b) \\ D_{BB} &= D_{0b} \left[1 - \bar{P}_b(\rho_s, \rho_b) + \rho_b \frac{\partial}{\partial \rho_b} \bar{P}_b(\rho_s, \rho_b) \right]. \end{aligned} \quad (8)$$

We denoted D_{0s} and D_{0b} are diffusion coefficients of pure system of small and big particles at infinite dilution, and similarly \mathbf{f}_{0s} and \mathbf{f}_{0b} drift of small and big particles at infinite dilution.

Besides the long-wavelength hydrodynamic limit we apply also mean-field approximation, neglecting correlations in occupation of neighbor sites. We addressed this question in our earlier work [43], where we investigated the generalized ASEP model with several types of particles. It was proved there that in the mean-field approximation, the probabilities of one-site configurations follow truncated Poisson distribution in the case of one type of particles, double truncated Poisson distribution in the case of two types of particles, etc. Therefore, we apply the multiple truncated Poisson distribution as the essence of the mean-field approximation we make.

Therefore, in this approximation, the probability of having n_s small and n_b big particles in one cell is given by double truncated Poisson distribution

$$P(n_s, n_b) = \frac{\lambda_s^{n_s} \lambda_b^{n_b}}{Z n_s! n_b!}, \quad (9)$$

where

$$Z(\lambda_s, \lambda_b) = \sum_{n_s=0}^k \sum_{n_b=0}^{[(k-n_s)/2]} \frac{\lambda_s^{n_s} \lambda_b^{n_b}}{n_s! n_b!} \quad (10)$$

is the partition function. The two parameters λ_s and λ_b of the double Poisson distribution, which belong to the small and big particles, respectively, fix the average densities. Borrowing a term from equilibrium statistical physics, we shall call the parameters λ_s and λ_b fugacities, keeping in mind that they are just numbers that parametrize the probability distribution.

There is a one-to-one correspondence between the pair of fugacities λ_s and λ_b and the pair of particle densities ρ_s

and ρ_b . Indeed, the fugacities determine the probability distribution of on-site particle configurations and this in turn determines the average densities. Therefore, we suppose that the dynamics in hydrodynamic limit can be formulated using time-and-position-dependent fugacities $\lambda_s(x, t)$ and $\lambda_b(x, t)$ instead of time-and-position-dependent densities $\rho_s(x, t)$ and $\rho_b(x, t)$. These two formulations are translated one to the other by the functions which express stationary and homogeneous densities through fugacities

$$\begin{aligned} \rho_s &= R_s(\lambda_s, \lambda_b) \equiv \lambda_s \frac{\partial \ln Z(\lambda_s, \lambda_b)}{\partial \lambda_s}, \\ \rho_b &= R_b(\lambda_s, \lambda_b) \equiv \lambda_b \frac{\partial \ln Z(\lambda_s, \lambda_b)}{\partial \lambda_b}. \end{aligned} \quad (11)$$

These formulas follow directly from the probabilities given by Eqs. (9) and (10).

In stationary state it leads to a great simplification. Indeed, as can be checked by insertion of Eqs. (11) and (8) into diffusion Eq. (7) with $\partial \rho_s / \partial t = \partial \rho_b / \partial t = 0$, the stationary state satisfies the equations for fugacities

$$\nabla \cdot \left[\left(\frac{R_\alpha^2(\lambda_s, \lambda_b)}{\lambda_\alpha(x)} \right) \left(D_{0\alpha} \frac{\nabla \lambda_\alpha(x)}{\lambda_\alpha(x)} - \mathbf{f}_{0\alpha} \right) \right] = 0. \quad (12)$$

The index $\alpha \in \{s, b\}$ denotes the particle type. Equations (12) are still coupled through the functions $R_\alpha^2(\lambda_s, \lambda_b)$, but do not contain cross-diffusion terms. This fact serves us as a basis for further calculations.

To avoid confusion, we also stress that at the same time as the hydrodynamic approximation is made, the particles become effectively pointlike. Therefore, no effects can occur stemming from the incommensurability of particle size and spatial period of the geometry, as it was observed in Ref. [72] and also in our earlier work [73].

III. TOY EXAMPLES: PIECEWISE ONE-DIMENSIONAL GEOMETRY

A. Simplifications in 1D

On a one-dimensional segment, the stationary currents of all types of particles are constants independent of position. This makes the one-dimensional geometry fundamentally different from higher dimensions. The diffusion equations formulated for fugacities (12) can be written as

$$j_\alpha \frac{\lambda_\alpha(x)}{R_\alpha^2(\lambda_s(x), \lambda_b(x))} = -D_{0\alpha} \frac{\partial \lambda_\alpha(x)}{\lambda_\alpha(x) \partial x} + f_{0\alpha}, \quad (13)$$

where j_α is the constant current of the particles of type α along the segment. Equations (13) are simplified with respect to Eq. (12) in the sense that they are of first order in spatial derivative. However, a serious complication remains here, namely the fact that the equations mix the dependence on all particle types through the functions $R_\alpha^2(\lambda_s(x), \lambda_b(x))$ which contain fugacities of all particle types as arguments. This complication is absent in two special situations we shall study in the following two subsections.

B. One type of particles in sawtooth potential

Equations (13) are particularly simple, if we allow just one type of particle. At the same time, the drift can be spatially

dependent. Thus, we have the equation

$$D_0 \frac{\partial \lambda(x)}{\lambda(x) \partial x} = f_0(x) - j \frac{\lambda(x)}{R^2[\lambda(x)]}. \quad (14)$$

We suppose the drift term has the form $f_0(x) = F - \frac{\partial V(x)}{\partial x}$, where F is constant external force and $V(x)$ is a periodic potential. As a simplest choice we use the sawtooth form

$$\begin{aligned} V(x) &= \frac{v}{L_+} x & \text{for } x \in (0, L_+), \\ V(x) &= -\frac{v}{L_-} x & \text{for } x \in (-L_-, 0), \end{aligned} \quad (15)$$

$$V(x + L_+ + L_-) = V(x) \quad \forall x.$$

In this case the drift is a piecewise constant function and this enables us to find the solution in terms of closed analytic formulas. The differential Eq. (14) together with the periodic condition $\lambda(-L_-) = \lambda(L_+)$ yields the pair of transcendental equations for the two fugacities $\lambda_0 \equiv \lambda(0)$ and $\lambda_1 \equiv \lambda(L_+)$

$$\begin{aligned} \int_{\lambda_1}^{\lambda_0} \frac{R^2(\lambda) d\lambda}{\left(\frac{v}{L_+} - F\right) \lambda R^2(\lambda) + j \lambda^2} &= \frac{L_+}{D_0}, \\ \int_{\lambda_1}^{\lambda_0} \frac{R^2(\lambda) d\lambda}{\left(\frac{v}{L_-} + F\right) \lambda R^2(\lambda) - j \lambda^2} &= \frac{L_-}{D_0}. \end{aligned} \quad (16)$$

When solved, we obtain the average particle density $\bar{\rho} = \int_{-L_-}^{L_+} \rho(x) dx / (L_- + L_+)$ as

$$\begin{aligned} \bar{\rho} &= \frac{D_0}{L_- + L_+} \int_{\lambda_1}^{\lambda_0} \left[\frac{1}{\left(\frac{v}{L_+} - F\right) \lambda R^2(\lambda) + j \lambda^2} \right. \\ &\quad \left. + \frac{1}{\left(\frac{v}{L_-} + F\right) \lambda R^2(\lambda) - j \lambda^2} \right] R^3(\lambda) d\lambda. \end{aligned} \quad (17)$$

We calculated the current-density diagram for the simplest case $k = 2$ where the function determining density in terms of fugacity is

$$R(\lambda) = \frac{\lambda + \lambda^2}{1 + \lambda + \frac{1}{2} \lambda^2}. \quad (18)$$

We show a typical behavior in Fig. 1. As expected, the density dependence of the current has a maximum. Although the detailed form of the current-density curve depends on parameters of the model like the force F and geometry determined by L_+ , L_- , the position of the maximum remains nearly unchanged. We also observe that for average density approaching either $\bar{\rho} \rightarrow 0$ or $\bar{\rho} \rightarrow 2$ the dependence is linear, because it corresponds to the regimes of nearly independent particles and nearly independent holes, respectively. However, when the density increases from zero, we observe enhancement of the current over the linear asymptotics. Such interaction-induced enhancement can be easily understood if we realize that free particles become partially trapped around the minimum of the potential $V(x)$, which leads to decrease in current. Such trapping is less severe for particles interacting by exclusion, because the effective capacity of the trap is limited by the exclusion principle. Indeed, for $k = 2$ we must have $\rho(x) \leq 2$ everywhere, including the neighborhood of the minimum of the potential, while for free particles $\rho(x)$

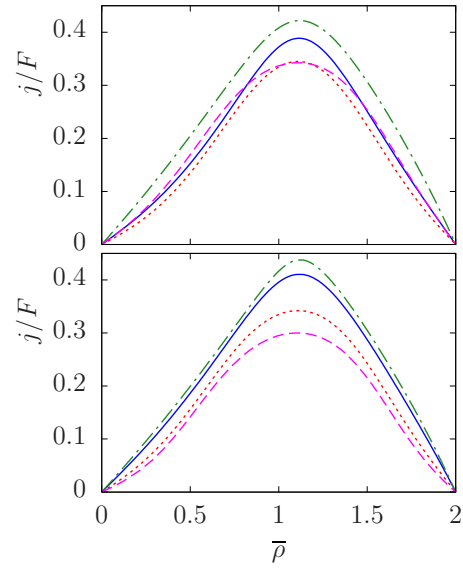


FIG. 1. Density dependence on the particle current in one-dimensional geometry with sawtooth potential (15) with parameters $k = 2$, $D_0 = 0.1$, $v = 0.5$. In the upper panel we use shape parameters $L_+ = 0.7$, $L_- = 0.3$ and force $F = 0.3$ (solid line), $F = -0.3$ (dotted line), $F = 0.6$ (dot-dashed line), and $F = -0.6$ (dashed line). In the lower panel we use force parameters $F = 0.5$ (solid line, dot-dashed line) and $F = -0.5$ (dashed line, dotted line) and shape $L_+ = 0.7$, $L_- = 0.3$ (solid line, dotted line) and $L_+ = 0.9$, $L_- = 0.1$ (dot-dashed line, dashed line).

can be arbitrarily large. Less particles trapped means more current, hence the superlinear increase of current for small densities. Analogous behavior is also observed close to the maximum density (which is 2 in this case), due to trapping of interacting holes. Although there is no particle-hole symmetry in this model, holes behave in a qualitatively similar manner as particles.

For $L_+ > L_-$ the “easy” direction of the flow under the influence of external driving F is positive, i.e., rightward. From Fig. 1 we can see that such intuitive reasoning holds true not just for nearly free particles, but at all densities. We observed, by varying the parameters of geometry as well as driving and diffusion coefficient, that this conclusion is generic. If we switch the external driving regularly between the values $|F|$ and $-|F|$, then the current averaged over many periods will exhibit the ratchet effect. For very slow switching the ratchet current is just the combination of stationary currents

$$J_{\text{rat}} = \frac{1}{2} (J_{F=|F|} + J_{F=-|F|}). \quad (19)$$

We show in Fig. 2 the ratchet current for several sets of the parameters of the model. As we already mentioned, the current is always larger in the “easy” direction, independently of the average density, so there is no current reversal at higher densities, contrary to the geometries we shall study later in this paper. Interesting feature, which we observed quite generically with the sawtooth potential, is the presence of two inflection points at intermediate densities. This is related to the already mentioned fact that the current behaves superlinearly both near the zero and near the maximum density. For small

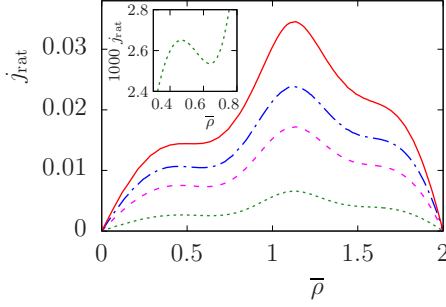


FIG. 2. Density dependence on the ratchet current in one-dimensional geometry with sawtooth potential (15). The diffusion coefficient is $D_0 = 0.1$ and the geometry parameter $v = 0.5$. The other parameters are $L_+ = 0.7$, $L_- = 0.3$, and $F = 0.3$ (dotted line), $L_+ = 0.7$, $L_- = 0.3$, and $F = 0.5$ (dashed line), $L_+ = 0.7$, $L_- = 0.3$, and $F = 0.6$ (dash-dotted line), $L_+ = 0.9$, $L_- = 0.1$, and $F = 0.5$ (solid line). In the inset, detail of the same data, for $L_+ = 0.7$, $L_- = 0.3$, and $F = 0.3$.

enough driving F , the effect may even lead to weak nonmonotonicity of the ratchet current, as shown in the inset of Fig. 2.

C. Two types of particles in pocket geometry

Another easily soluble case corresponds to particles in the pocket geometry sketched in Fig. 3. On a straight line (we shall call it backbone), at regularly spaced points at distance L of each other, tilted segments of length W are attached. These segments represent dead ends, so that no current can flow through them in stationary state, but they act as traps accumulating certain portion of particles, thus reducing the current along the backbone. We shall call these segments pockets.

The pockets are tilted to the left at angle α . This has the effect that if the drift due to external field is f on the backbone, it is $-f \cos \alpha$ on the pocket. The geometry is not strictly one-dimensional, but it is piecewise one-dimensional, as it is composed by linear segments joined at discrete points. therefore, we can use the general Eq. (13) on each segment separately and then guarantee appropriate gluing at the joints, by imposing proper boundary conditions at the ends of each segment.

The fact that no current flows through the pockets makes the Eq. (13) particularly simple inside the pockets, namely

$$\begin{aligned} D_{0s} \frac{\partial \lambda_s(x)}{\lambda_s(x) \partial x} &= -f_{0s} \cos \alpha, \\ D_{0b} \frac{\partial \lambda_b(x)}{\lambda_b(x) \partial x} &= -f_{0b} \cos \alpha. \end{aligned} \quad (20)$$

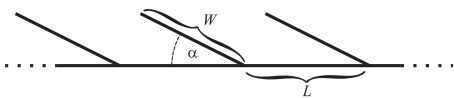


FIG. 3. Scheme of the pocket geometry. On a straight line (backbone) at regular distances L , segments of length W are attached (pockets). The pockets are tilted at angle α .

We denoted f_{0s} and f_{0b} the drift at infinite dilution on the backbone for small and big particles, respectively, and we have taken into account tilting of the pockets as shown in Fig. 3. The coordinate x parametrizes the position on the pocket, starting with $x = 0$ at the joint with the backbone and increasing toward $x = W$ at the end of the pocket.

Technically, the most important point is that the fugacities for small and big particles decouple, so each equation of the pair (20) can be solved separately. The exponential dependence, or barometric formula, which holds for densities in the case of noninteracting particles, holds for fugacities when interaction is taken into account by our hydrodynamic approximation. Therefore,

$$\begin{aligned} \lambda_s(x) &= \lambda_{s0} e^{-x f_{0s} \cos \alpha / D_{0s}}, \\ \lambda_b(x) &= \lambda_{b0} e^{-x f_{0b} \cos \alpha / D_{0b}}. \end{aligned} \quad (21)$$

The average densities and currents (which flow along the backbone) depend on just two parameters, namely the fugacities $\lambda_{s0} \equiv \lambda_s(0)$ and $\lambda_{b0} \equiv \lambda_b(0)$. Of course, the densities, and therefore also the fugacities, are constant throughout the backbone and these uniform values are equal to the boundary value at $x = 0$ for the pockets. We obtain

$$\begin{aligned} \bar{\rho}_s &= \frac{LR_s(\lambda_{s0}, \lambda_{b0}) + \int_0^W R_s(\lambda_s(x), \lambda_b(x)) dx}{L + W}, \\ \bar{\rho}_b &= \frac{LR_b(\lambda_{s0}, \lambda_{b0}) + \int_0^W R_b(\lambda_s(x), \lambda_b(x)) dx}{L + W} \end{aligned} \quad (22)$$

for the average densities of small and big particles, respectively, where the dependence of fugacities on the coordinate x along the pocket is given by Eq. (21). For the currents, we obtain simple formulas

$$\begin{aligned} j_s &= f_{0s} \frac{R_s^2(\lambda_{s0}, \lambda_{b0})}{\lambda_{s0}}, \\ j_b &= f_{0b} \frac{R_b^2(\lambda_{s0}, \lambda_{b0})}{\lambda_{s0}}. \end{aligned} \quad (23)$$

We focused on the specific case $k = 3$, where

$$\begin{aligned} R_s(\lambda_s, \lambda_b) &= \frac{\lambda_s + \lambda_s^2 + \frac{1}{2}\lambda_s^3 + \lambda_s \lambda_b}{1 + \lambda_s + \frac{1}{2}\lambda_s^2 + \frac{1}{6}\lambda_s^3 + \lambda_b + \lambda_s \lambda_b}, \\ R_b(\lambda_s, \lambda_b) &= \frac{\lambda_b + \lambda_s \lambda_b}{1 + \lambda_s + \frac{1}{2}\lambda_s^2 + \frac{1}{6}\lambda_s^3 + \lambda_b + \lambda_s \lambda_b}. \end{aligned} \quad (24)$$

Especially, we are interested in how the geometry, i.e., the length and angle of inclination of the pockets, influences the stationary current along the backbone. In Figs. 4 and 5 we show the dependence of the currents of small and big particles on the average density of small particles, with average density of big particles fixed. Having in mind the ratchet effect, we plot the results for both orientations of the driving, i.e., for $f_0 = |f_0|$ and for $f_0 = -|f_0|$. In all these results we assume that both diffusion coefficient and drift of big particles are half of those of small particles. This way we take into account the fact that transport coefficients are inversely proportional to particle size. Therefore, $D_{0s} = D_0$, $D_{0b} = D_0/2$, $f_{0s} = f_0$, and $f_{0b} = f_0/2$.

In Fig. 4 we compare results for several lengths W of the pocket. Let us first look at the current of small particles. As

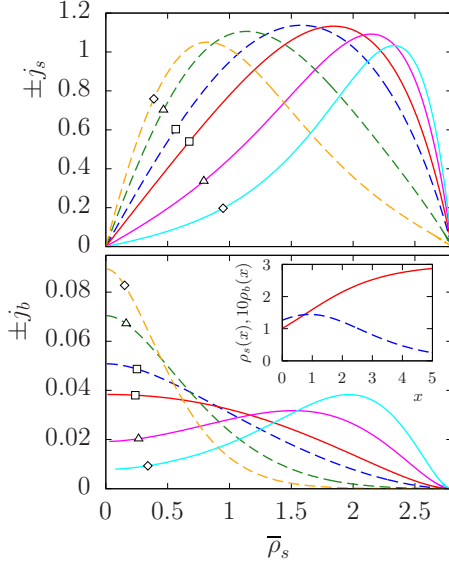


FIG. 4. Dependence of the current of small (upper panel) and big (lower panel) particles on the average density of small particles, for average density of big particles $\bar{\rho}_b = 0.1$. The transport parameters are $f_0 = 1$, $D_0 = 1$ and geometry parameters $L = 1$, $\cos \alpha = 0.7$. The dashed lines correspond to the “+” sign in front of j_s and j_b (i.e., positive current), solid lines correspond to the “-” sign in front of j_s and j_b (i.e., negative current). The lines are marked by symbols which correspond to parameters $W = 1$ (\square), $W = 3$ (\triangle), and $W = 5$ (\diamond). In the inset in the lower panel, local density of small (solid line) and big (dashed line) particles within the pocket. The transport parameters are $f_0 = -1$, $D_0 = 1$, the geometry parameters are $L = 1$, $W = 5$, $\cos \alpha = 0.7$, and the average densities $\bar{\rho}_s = 2$ and $\bar{\rho}_b = 0.1$.

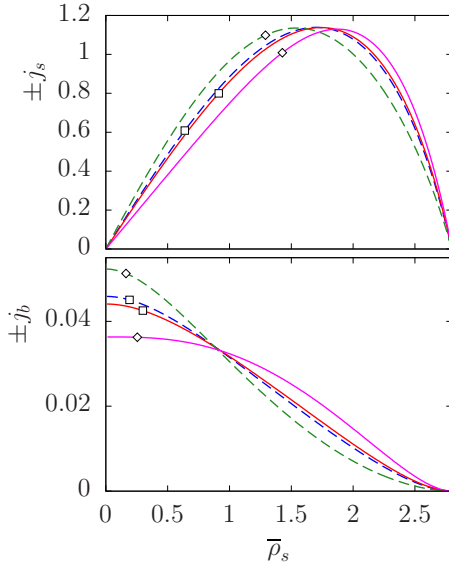


FIG. 5. Dependence of the current of small (upper panel) and big (lower panel) particles on the average density of small particles, for average density of big particles $\bar{\rho}_b = 0.1$. The transport parameters are $f_0 = 1$, $D_0 = 1$ and geometry parameters $L = 1$, $W = 1$. The dashed lines correspond to the “+” sign in front of j_s and j_b (i.e., positive current), solid lines correspond to the “-” sign in front of j_s and j_b (i.e., negative current). The lines are marked by symbols which correspond to parameters $\cos \alpha = 0.1$ (\square) and $\cos \alpha = 0.9$ (\diamond).

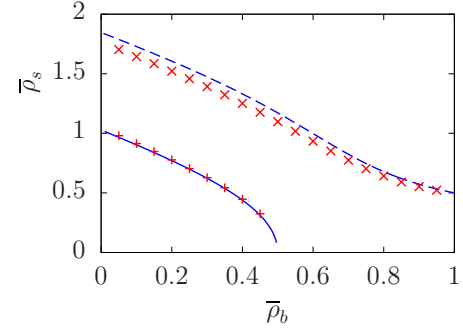


FIG. 6. Phase diagram of the ratchet currents of small and big particles in the pocket geometry with parameters $L = 1$, $W = 1$, $\cos \alpha = 0.7$, $D_0 = 1$. The region of full separation, i.e., when the ratchet current of small particles is positive, while the ratchet current of big particles is negative, is delimited by a pair of lines $\bar{\rho}_{sc2}(\bar{\rho}_b)$ and $\bar{\rho}_{sc1}(\bar{\rho}_b)$. Two pairs of lines are shown for two different forces f_0 . For $f_0 = 1$ it is the pair of solid line (from below) and dashed line (from above). For $f_0 = 5$ the shapes of the lines in the pair are indicated by symbols \times indicate the line delimiting the region from above, the symbols $+$ indicate the line delimiting the region from below. Note that the lower lines nearly coincide for $f_0 = 5$ and $f_0 = 1$, while the upper lines slightly differ for this two values of f_0 .

expected, the “easy” direction is positive, i.e., rightward, as long as $\cos \alpha > 0$. This means that for small $\bar{\rho}_s$ the absolute value of the current is larger for $f_0 = |f_0|$ than for $f_0 = -|f_0|$. However, contrary to the case of sawtooth potential investigated in the previous section, in the pocket geometry this holds only for densities $\bar{\rho}_s < \bar{\rho}_{sc1}$. At the critical density $\bar{\rho}_{sc1}$ the ratchet current of small particles changes sign. This can be described by saying that the “easy” direction for holes is opposite to the “easy” direction for particles. Similar picture holds also for big particles. The ratchet current is positive for $\bar{\rho}_s < \bar{\rho}_{sc2}$ and negative beyond the second critical density $\bar{\rho}_{sc2}$. For the data shown in Fig. 4 we observe that $\bar{\rho}_{sc2} < \bar{\rho}_{sc1}$. Therefore, there is an interval of densities $\bar{\rho}_s \in (\bar{\rho}_{sc2}, \bar{\rho}_{sc1})$ where ratchet current of small particles is positive, while ratchet current of big particles is negative. Figure 4 shows the situation for just one fixed value of the density of big particles $\bar{\rho}_b$. For other values of $\bar{\rho}_b$ the critical densities $\bar{\rho}_{sc2}$ and $\bar{\rho}_{sc1}$ may change or even disappear. We can display the situation by a phase diagram in the axes $\bar{\rho}_s$ and $\bar{\rho}_b$. The two critical densities, as functions of $\bar{\rho}_b$, i.e., $\bar{\rho}_{sc2}(\bar{\rho}_b)$ and $\bar{\rho}_{sc1}(\bar{\rho}_b)$, define lines which delimit the region of densities for which the ratchet currents of small and big particles have opposite sign (we shall call it region of full separation). In this region we have $\bar{\rho}_{sc2}(\bar{\rho}_b) < \bar{\rho}_s < \bar{\rho}_{sc1}(\bar{\rho}_b)$. We show the phase diagram in Fig. 6 for two sets of parameters. As we can see, the region of full separation forms a diagonal band extending from big $\bar{\rho}_s$ and small $\bar{\rho}_b$ to big $\bar{\rho}_b$ and small $\bar{\rho}_s$. If we imagine a device intended for separation of big particles from small particles in a mixture using ratchet effect in our pocket geometry, then it indeed separates the two types of particles perfectly, as long as the densities remain in the region of full separation. The diagonal shape of the region means, that during the separation process the densities of small and big particles may

in principle evolve so that they remain all the time in the region of full separation and at the end all big particles are accumulated at one end and all small particles at the opposite end of the device. Of course, practical application of such scenario would require significant amount of fine tuning of the apparatus.

In Fig. 6 we can also see that increasing the driving force from $f_0 = 1$ to $f_0 = 5$ has only very small influence on the shape of the region of full separation. If we look back to Fig. 4, we observe that the critical densities $\bar{\rho}_{sc2}$ and $\bar{\rho}_{sc1}$ depend very little on the geometric parameter W (the length of the pocket). The shape of the curves j_s and j_b as functions of $\bar{\rho}_s$ varies significantly when we increase W , but the density at which the two curves corresponding to positive and negative f_0 cross, remains nearly the same. Similar conclusion can be deduced from Fig. 5, where the current is shown for several inclinations α of the pocket. Again, the current itself does depend on the angle α , but the critical densities remain nearly unchanged. All these observations imply that the shape of the region of full separations, as shown in Fig. 6 is very robust and nearly independent of the details of the geometry and of the strength of the driving f_0 . Let us also note that a phase diagram very similar to Fig. 6 was obtained in our previous work [43] where we studied a discrete model by direct numerical simulations.

Let us turn once more to Fig. 4. For $W = 1$ the dependence of j_s on $\bar{\rho}_s$ is concave, but for $W = 3$ inflection point appear and this is even more pronounced for $W = 5$. It corresponds to enhancement of the particle current over the linear dependence. We observed this phenomenon on the previous section in the model with sawtooth potential (see Fig. 1). The explanation is again the same. Indeed, repulsive interaction between particles prevents them from filling the pockets beyond the maximum density, therefore more particles remain on the backbone and these extra particles are responsible for the interaction-induced enhancement of the current. A bit more subtle is the effect observed in the dependence of the current of big particles on $\bar{\rho}_s$. For negative, i.e., leftward driving, $f_0 < 0$, and for $W = 3$ and $W = 5$, we observe that the current of big particles increases when density of small particles increases. This seems counterintuitive, as one would guess that small particles act as obstacles for the movement of big ones. However, the actual scenario is more tricky. The small particles quickly fill the pockets thus forcing the big particles to remain in the backbone. This is illustrated in the inset in Fig. 4. We can see how the densities of small and big particles depend on the position inside the pocket. The driving is $f_0 = -1$, i.e., the particles are pushed into the pocket. While the density of small particles increases monotonously when we proceed from the entrance to the end of the pocket, the big particles behave differently. Initially, their density increases a little, but when we proceed deep inside the pocket, the density of big particles decreases substantially. Small particles push the big ones out of the pocket, countering and reversing the effect of the driving force. As a result, the current of big particles is enhanced. Note that this is analogous to the Brazil nut phenomenon, occurring frequently in shaken mixtures of granular matter [74]. We shall encounter this effect at several occasions later.

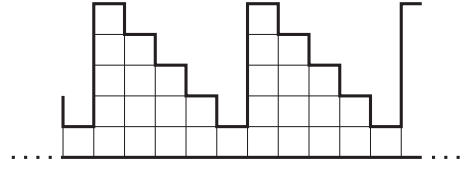


FIG. 7. Scheme of the two-dimensional channel geometry. The channel is composed of periodically repeating teeth, each tooth consisting of 15 squares drawn by the thin lines. The edges of the squares have unit length. In the continuous description, the position of the particles can be anywhere within the area delimited by the borders shown as the thick lines. In the discrete description, the number of particles within each square must satisfy the condition (25).

IV. TWO-DIMENSIONAL CHANNELS

A. Geometry

Let us now turn to more realistic geometries. In this section we shall consider channels with periodically varying profile in the horizontal direction, but with uniform height in the vertical direction, comparable with the size of the particles. Therefore, the movement of the particles can be considered effectively two-dimensional. Such structures are routinely fabricated using PDMS soft lithography [9,75] and this is the experimental situation we have in mind in our theoretical modeling.

We shall investigate the dynamics of particles in 2D channel with geometry sketched in Fig. 7. The channel consists of a series of identical teeth. Each tooth is composed of 15 equal square cells. The edge of a single square sets the unit of length.

B. Discrete model

In the discrete formulation we performed Monte Carlo simulations of the generalized ASEP model in the geometry shown in Fig. 7. The dynamical variables are the numbers of particles in each of the square cells which must obey the exclusion constraint (5). Specifically, each square cell has capacity $k = 3$, there are just two types of particles (small and big). The small particles have size factor $c_s = 1$, the big ones have $c_b = 2$. Therefore, in each cell the number of small particles n_s and big particles n_b must satisfy the constraint

$$n_s + 2n_b \leq k. \quad (25)$$

The sets of hopping rates are, in the direction right, left, up, down, respectively, denoted a, b, c, d for small particles and A, B, C, D for big particles. We always fix $c = d, C = D$. To keep compatibility with continuous description, the free diffusion coefficients and drifts are $D_{0s} = (a + b)/2 = (c + d)/2$, $f_{0s} = a - b$ for small particles and $D_{0b} = (A + B)/2 = (C + D)/2$, $f_{0b} = A - B$ for big particles. Moreover, as the properties of Brownian motion imply that the diffusion coefficient and mobility are both inversely proportional to particle radius, we fix the relation between the hopping rates of small and big particles as $A = a/2, B = b/2, C = c/2$, and $D = d/2$. Therefore, there are just two free parameters of the model, namely $D_0 \equiv D_{0s}$ and $f_0 \equiv f_{0s}$. The average density of particles of type α is $\bar{\rho}_\alpha = N_\alpha/(15L)$, where L is the number of teeth in

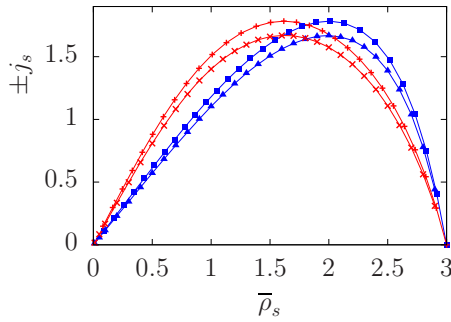


FIG. 8. Particle current in the one-component system (small particles only) in the two-dimensional teeth geometry shown in Fig. 7. The diffusion coefficient is $D_0 = 1$ and the driving $f_0 = 1$ (symbols $+$ and \times and sign “+” in front of j_s) and $f_0 = -1$ (symbols \blacksquare and \blacktriangle and sign “-” in front of j_s). The points show the results of the Monte-Carlo simulation of the discrete model (symbols \times and \blacktriangle) and solution of the Eq. (12) using COMSOL software in the continuous formulation (symbols $+$ and \blacksquare).

the sample, each comprising 15 cells, and N_α the number of particles of type α in the simulation.

C. Continuous formulation in hydrodynamic approximation

In the continuous formulation, we solved numerically the set of Eq. (12) in stationary state in the channel delimited by thick lines in the scheme shown in Fig. 7. We fix the x axis along the channel and y axis perpendicular to it. Consistently with the discrete formulation, there are just two types of particles, and we consider the simplest nontrivial case $k = 3$. The functions $R_\alpha(\lambda_s, \lambda_b)$ are given by the formulas (24). To keep the transport coefficients consistent with the discrete model, we fix the diffusion coefficients $D_{0s} = 2D_{0b} = D_0$ and drift $f_{0s} = 2f_{0b} = f_0$. The boundaries (thick lines) impose reflecting boundary conditions. The teeth repeat periodically, so that we impose periodic conditions on the fugacities $\lambda_\alpha(x + 5, y) = \lambda_\alpha(x, y)$, as each tooth has length 5 in the x direction. The numerical solution is performed using the COMSOL software. The average density of particles of type α is just the integral of the local density over one tooth divided by the area of the tooth, $\bar{\rho}_\alpha = \int_{\text{tooth}} \rho_\alpha(x, y) dx dy / 15$.

D. Comparison

First, we studied the one-component system with small particles only. We show in Fig. 8 the current of particles as a function of average density. As expected, we observe the maximum of the current, which lies at different position depending on the sign of the drift f_0 . When the orientation of the drift is switched periodically, a ratchet effect occurs. If the frequency of switching is very small, then we may use the adiabatic approximation and calculate the ratchet current as arithmetic mean of the currents for $f_0 = |f_0|$ and $f_0 = -|f_0|$. The ratchet current calculated in such a way can be grasped from Fig. 8 directly. We can see that in the geometry of Fig. 7 the ratchet current is positive for small densities, corresponding to the easy direction toward the right. At a density around $\bar{\rho}_s \simeq 1.8$ the ratchet current changes sign and becomes negative. Recall that the change of sign of the ratchet current is absent in the

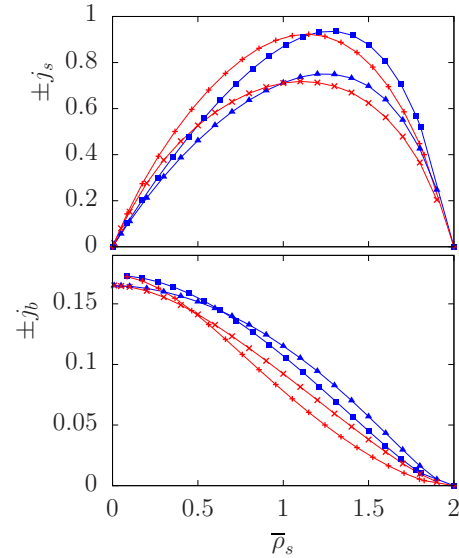


FIG. 9. Current of the small (upper panel) and big (lower panel) particles in the two-dimensional teeth geometry shown in Fig. 7. The diffusion coefficient is $D_0 = 1$ and the driving $f_0 = 1$ (symbols $+$ and \times and sign “+” in front of j_s) and $f_0 = -1$ (symbols \blacksquare and \blacktriangle and sign “-” in front of j_s). The average density of big particles is $\bar{\rho}_b = 0.5$. The points show the results of the Monte-Carlo simulation of the discrete model (symbols \times and \blacktriangle) and solution of the set of Eq. (12) using COMSOL software in the continuous formulation (symbols $+$ and \blacksquare).

one-dimensional model investigated in the last section, but occurs in the pocket geometry. This indicates that the pocket geometry indeed grasps essential features of the 2D systems.

Comparing the results of discrete and continuous approaches, we can see that the hydrodynamic approximation slightly overestimates the current, but the difference remains rather small. Moreover, it is interesting to note that the density at which the ratchet current changes sign is nearly equal for the discrete and continuous formulations. All of this suggests that the hydrodynamic approximation is fairly reliable for one-component colloid suspensions.

Next we simulated the mixed system of small and big particles. We show in Fig. 9 how the current of small and big particles depend on the average density of small particles, with average density of big particles fixed. As expected, we can observe the maximum in the current of small particles and monotonous decrease in the current of big particles. Similarly to one-component system, comparison of the results for positive and negative drift tells us what is the ratchet current like in adiabatic approximation. Again, we observe current reversal in the ratchet current of small particles. The current reversal for big particles is absent in Fig. 9, but this is a special feature of the particular choice of the density of big particles $\bar{\rho}_b = 0.5$. For a generic $\bar{\rho}_b$, also the current of big particles exhibits the change of sign. Thus, also the mixed system of small and big particles is qualitatively very close when we compare the piecewise-one-dimensional pocket geometry and the two-dimensional tooth geometry.

Comparing the results for the discrete and continuous models, we can see that the agreement is significantly worse

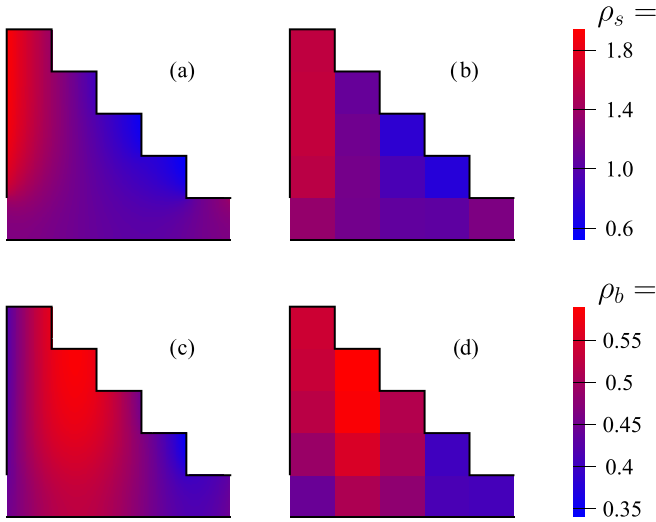


FIG. 10. Local densities of small (a, b) and big (c, d) particles, obtained from continuous formulation (a, c) and from discrete model (b, d) in the two-dimensional teeth geometry shown in Fig. 7. The transport coefficients are $D_0 = 1$, $f_0 = -1$. The average density of small particles is $\bar{\rho}_s = 1.2$ and the average density of big particles is $\bar{\rho}_b = 0.5$. The color encoding for the local densities is given by the legends on the right-hand side.

than in the case of one-component system, although qualitatively the behavior remains comparable. Such observation is consistent with the results we obtained recently [45] on one-dimensional generalized ASEP model. Indeed, in Ref. [45] we showed that the mean-field and Kirkwood approximations are excellent for one-component system, but become quantitatively off by several tens of percent if we work with two-component system. In Ref. [45] we identified the source of the disagreement to be long-range correlations which develop due to indirect interaction of one type of particles mediated by the other type of particles. We believe that the same mechanism is responsible for the difference between discrete and continuous models also here.

In Fig. 10 we can see the spatial distribution of small and big particles within one tooth. The orientation of the drift is leftward and this corresponds to marked accumulation of small particles at the left edge of the tooth. On the contrary, big particles are localized mostly near the middle of the tooth. This is another manifestation of the phenomenon analogous to Brazil nut effect. Indeed, small particles accumulated next to the left edge of the tooth prevent the big particles from entering the leftmost region. The big particles, which are also *a priori* pushed leftward, remain at a half way. This phenomenon can be seen in both discrete and continuous models. Also other details of the local density are very similar in discrete and continuous variants, so we can conclude that the continuous description works well in terms of spatial distribution of the particles.

V. THREE-DIMENSIONAL GEOMETRIES

A. Mixture of particles in a container: The Brazil nut effect

In static case, i.e., with strictly zero current everywhere, the equations for fugacities (12) decouple. For example, we

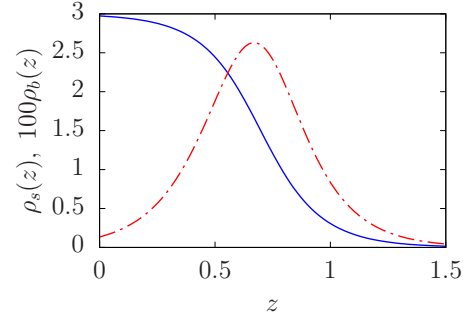


FIG. 11. The Brazil nut effect: local densities of small (solid line) and big (dot-dashed line) particles in a cylinder of height $h = 1.5$ with vertical axis along the z coordinate. The average densities are $\bar{\rho}_s = 1.4$ for small particles and $\bar{\rho}_b = 0.01$ for big particles. The transport coefficients are $D_0 = 1$, $f_0 = 6$.

consider a mixture of two types of particles in a cylindrical container, with vertical axis, under influence of gravity. We identify the vertical direction with the z axis and we have homogeneous field $f_{0x} = f_{0y} = 0$, $f_{0z} = -f_0$. The solution of Eq. (12) is trivial,

$$\begin{aligned}\lambda_s(x, y, z) &= \lambda_{s_0} e^{-\frac{f_0}{D_0} z}, \\ \lambda_b(x, y, z) &= \lambda_{b_0} e^{-\frac{f_0}{D_0} z},\end{aligned}\quad (26)$$

and the densities of particles are deduced directly from Eq. (26) using the functions (24) as

$$\begin{aligned}\rho_s(x, y, z) &= R_s(\lambda_{s_0} e^{-\frac{f_0}{D_0} z}, \lambda_{b_0} e^{-\frac{f_0}{D_0} z}), \\ \rho_b(x, y, z) &= R_b(\lambda_{s_0} e^{-\frac{f_0}{D_0} z}, \lambda_{b_0} e^{-\frac{f_0}{D_0} z}).\end{aligned}\quad (27)$$

We show in Fig. 11 the typical density profile of small and big particles. In this example we assume that there are just few big particles, i.e., the average concentration of big particles is much smaller than the concentration of small ones. The small particles accumulate at the bottom, with diffuse but steep drop of density around a depth analogous to a “liquid level.” Then, the big particles accumulate around this “liquid level,” thus resembling big particles floating on the top of the bulk of small particles. This is just what is observed in the Brazil nut phenomenon. However, there is a fundamental difference. In the Brazil nut experiments [74], one uses shaken granular material, while in our model, we deal with Brownian particles under the influence of thermal fluctuations.

In this formulation, the Brazil nut effect occurs in a static regime with no macroscopic current. As we have seen in the last two sections, it can be observed also in nonequilibrium situations. So, we can conjecture that it is a generic feature of mixed systems of small and big particles.

B. Axially symmetric pore

Now we consider the mixture of small and big particles inside an axially symmetric pore, with driving parallel to the axis. We use cylindrical coordinates with axis z coinciding with the axis of the pore and radial coordinate r . All quantities will be symmetric with respect to rotation around the axis, so the dependence on the azimuthal angle ϕ is absent. The pore is

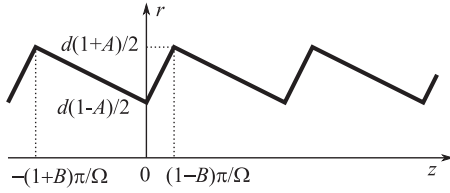


FIG. 12. The profile of the axially symmetric pore. The z axis coincides with the axis of the pore. The geometry is characterized by parameters d (average diameter), Ω (spatial frequency), A (depth of the profile), and B (asymmetry of the profile).

delimited by a periodic wall, $r < h(z)$, $h(z) = h(z + 2\pi/\Omega)$. For simplicity, we shall use a sawtooth-type boundary, as sketched in Fig. 12. There are three geometric parameters, d specifying the average diameter of the pore, Ω the spatial frequency, A depth of the profile, and B asymmetry of the profile. Specifically, we have

$$h(z) = \frac{d}{2} \left(1 + A \left(\frac{2z}{z_1} - 1 \right) \right), \quad z \in (0, z_1),$$

$$h(z) = \frac{d}{2} \left(1 - A \left(\frac{2z}{z_2} + 1 \right) \right), \quad z \in (-z_2, 0), \quad (28)$$

where we denoted $z_1 = (1 - B)\pi/\Omega$ and $z_2 = (1 + B)\pi/\Omega$.

We solved the transport Eq. (12) using the COMSOL software. From a technical point of view, the axial symmetry facilitated substantially the numerical solution. In Fig. 13 we show the current of small and big particles as a function of the average density of small particles. Comparing the results for rightward and leftward driving, we can immediately infer the properties of the ratchet current in adiabatic approximation (i.e., when periodic flipping of the orientation of the drift

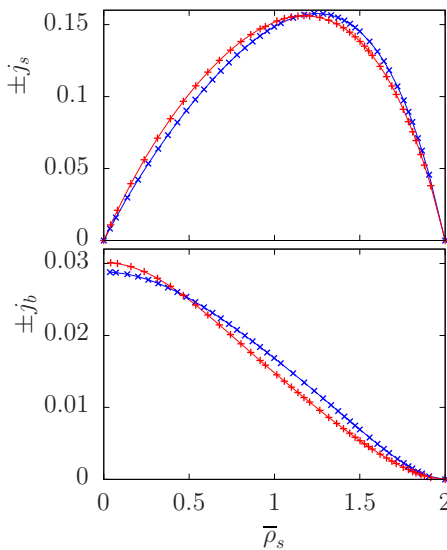


FIG. 13. Current of small (upper panel) and big (lower panel) particles in axially symmetric pore with geometry defined by Eq. (28). The geometric parameters are $d = 0.3$, $\Omega = 20$, $A = 0.3$, $B = 0.8$, the transport coefficients are $D_0 = 0.2$, $f_0 = 5$ (symbols +, sign “+” in front of j_a and j_b) and $f_0 = -5$ (symbols \times , sign “-” in front of j_a and j_b). The average density of big particles is $\bar{\rho}_b = 0.5$.

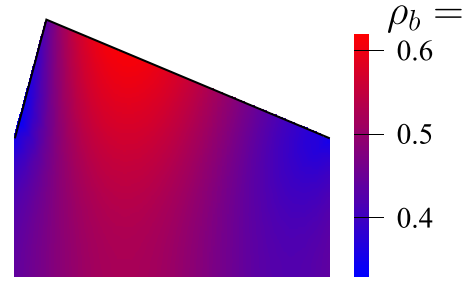
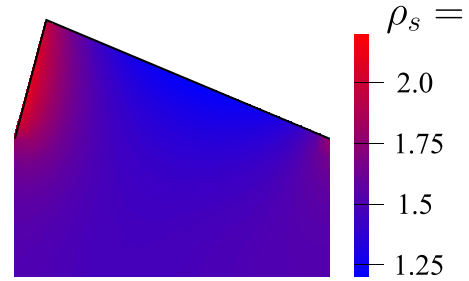


FIG. 14. Spatial distribution of the particle densities for small particles (upper panel) and big particles (lower panel) inside one spatial period of the pore with profile defined by Eq. (28). The color encoding for local densities is given by the legends on the right-hand side. The geometric parameters are $d = 0.3$, $\Omega = 20$, $A = 0.3$, $B = 0.8$, the transport coefficients are $D_0 = 0.2$, $f_0 = -5$, and the average particle densities are $\bar{\rho}_s = 1.5$, $\bar{\rho}_b = 0.5$.

occurs very slowly). We can see that the ratchet current of both small and big particles is positive if the density of small particles is small enough. This corresponds to moving in the easy direction dictated by the geometry sketched in Fig. 12. Indeed, the easy direction is rightward as long as the asymmetry parameter $B > 0$, which is the case for the data in Fig. 13. When the density of small particles increases, the ratchet current of big particles becomes negative first and the ratchet current of small particles later. This means that there is an interval of densities $\bar{\rho}_s$ in which the ratchet effect carries the small and big particles in opposite directions, thus enabling full separation of the particle types. This is the same effect as observed already in the piecewise one-dimensional geometry with pockets, studied in Sec. III C. Also the whole current-density diagram of a 3D system, Fig. 13, is qualitatively very similar to corresponding diagram for pocket geometry, Fig. 5. This indicates that the pocket geometry, when properly calibrated, can bring useful information even on the behavior of 3D systems. We would like to consider that a late justification of our earlier studies of generalized ASEP models in pocket geometry presented in our previous work [43].

We also looked at the detailed distribution of densities of small and big particles in the pore. Due to the symmetry, the density depends only on the axial and radial coordinates. Thus, we show in Fig. 14 the densities in a plane containing the axis of the pore. We also assume periodicity of the density along the axis and show just one spatial period of the pore. In the case shown in Fig. 14 the drift goes leftward and we can see accordingly the accumulation of small particles at the left wall of the pore. The big particles, however, are concentrated

around the middle of the period, manifesting once again the Brazil nut phenomenon. Indeed, the spatial distributions of particles in 3D geometry in Fig. 14 and in 2D geometry in Fig. 10 are qualitatively very similar.

VI. CONCLUSIONS

We formulated a hydrodynamic approximation for movement of dense colloidal suspension of Brownian particles. The formulation goes in two steps, first approximating the true Brownian motion with steric repulsion of particles by a discrete stochastic model, the generalized asymmetric exclusion process (ASEP), and then performing hydrodynamic limit in this generalized ASEP model. The approximation is formulated for mixtures of particles of various types, differing by size, diffusion coefficient and drift. In practical calculation, we worked with just two types of particles (we called them small particles and big particles). An important feature of our approach is that the transport equations are formulated in terms of fugacities corresponding to the particle types, rather than in terms of particle densities. In such formulation, there are situations in which the equations for several particle types decouple and each particle type can be treated independently. We investigated several such situations.

We studied the model in one-, two-, and three-dimensional geometries. In a truly 1D system, we placed the driven one-component system (small particles only) on a line under the influence of periodic sawtooth potential. In this case, the transport equation can be solved explicitly. We observed several interesting features of the dependence of current on average density. For small densities, current grows faster than linearly with density of particles. At certain density the current reaches a maximum and then decreases when the density approaches its maximum dictated by the cell capacity. Close to the maximum density, we can look at the current-density diagram as showing the dependence of current on the density of holes. Again, we observe that the current increases faster than linearly with the density of holes. This superlinear behavior at both low and high densities can be easily interpreted as a consequence of steric repulsion of particles. Indeed, noninteracting particles accumulate near the minima of the sawtooth potential. This leads to suppression of the current, because particles trapped at the minimum must overcome a potential barrier. Steric repulsion puts a limit to the accumulation of particles anywhere, therefore less particles are located at the minima and the spatial distribution of particle density is more uniform. Hence, less particles are slowed down by the potential barrier and the current may be higher.

We also studied the piecewise one-dimensional case of pocket geometry. In this setting, linear segments (called pockets) are appended at regularly spaced points to a straight line. In stationary state the current is constant and nonzero only on the straight line, while it is zero in the pockets. This is one of the cases when transport equations for different types of particles decouple and are solved independently. In this case, the solution of the equations is particularly easy. In fact, the spatial dependence of fugacities for both small and big particles follow the barometric formula, familiar from the problem of free Brownian particles in static gravitational field. From this observation we deduced the current-density diagram for

both types of particles and density dependence of the ratchet currents in adiabatic approximation. In this case, the ratchet current changes sign at certain value of the density. There is a region of densities in which the ratchet currents of small and big particles are oriented in opposite direction, therefore enabling (in principle) perfect separation of the two particle types. In the two-dimensional diagram with densities of small and big particles on horizontal and vertical axes, respectively, we can identify the region where the ratchet currents point in opposite side. Interestingly, this region forms a strip going diagonally from pure small particles to pure big particles. This indicates that we can start with a mixture of small and big particles and separating gradually the one from the other, we can achieve full separation, as long as we remain, during the process, all the time within the strip. Note that similar diagram was obtained by simulations of generalized ASEP model in our previous work [43].

In this work we limited our study of the ratchet effect to adiabatic approximation. In reality, however, the direction-switching frequency is finite and represents an important parameter of the experimental setup. It would be in principle straightforward to extend our analysis to arbitrary time-dependent driving by solving the full time-dependent nonlinear diffusion Eq. (7). However, currently we do not see a way to obtain analytic results and the only way would be numerical solution. This could not be complicated using the COMSOL software but we leave it for future work. We expect that the ratchet current would be a decreasing function of frequency, ultimately approaching zero for very fast switching. However, we cannot exclude a stochastic resonance leading to a maximum current at finite frequency. This question must be answered by a specific detailed computation.

In a two-dimensional geometry, we placed the particles in a periodic tooth-shaped channel. We compared the continuous hydrodynamic description with simulation of discrete generalized ASEP model in the same geometry. The results are quantitatively close to each other. In the case of one-component system (small particles only), the agreement is very good. However, for mixed small and big particles, the agreement worsens, as the continuous description cannot take into account complicated long-range correlations. This is similar to our observation we made in our recent work on generalized ASEP model [45].

However, the continuous hydrodynamic description correctly describes one important phenomenon involving correlations between small and big particles, which is the Brazil nut effect. It is manifested in depletion of big particles from the areas where small particles concentrate. For example, it implies that the driven small particles in the tooth-shaped channel accumulate at the posterior walls of the teeth, as expected, but the big particles are mostly located around the middle of each tooth, rather than at the posterior wall. The reason is that the small particles accumulate easily and the big particles do not find enough space at places occupied already by small ones. In this respect, the discrete and continuous descriptions are in full accord. This may be understood well, because the Brazil nut phenomenon reflects purely local correlations. Such correlations are well described by the continuous theory, contrary to the long-range correlations, as shown by us also in Ref. [45].

We also looked at truly three-dimensional, though simplified, geometries. We investigated explicitly the Brazil nut effect, mentioned earlier, in static case of the mixture of small and big particles in a cylindrical container in homogeneous axial external field. The external field can be viewed as gravitational force. Then, the small particles are concentrated at the lower part of the container, resembling a liquid in a half-filled bottle, while the big particles look as if they floated on top of the surface of the small-particle liquid. Note, however, that the real experiments with the Brazil nut phenomenon [76–78] are made with shaken granular matter of two different sizes of grains, while our theory works with Brownian particles agitated by thermal fluctuations. There is no trivial correspondence between these two situations, but rather just an analogy. The Brazil nut effect in shaken granular mixtures was amply studied by molecular dynamics (e.g., Refs. [78–80]) or schematic Monte Carlo simulations (e.g., Ref. [74]). These studies take into account many more details of the process than our method, but comparison of stationary density profiles (e.g., Ref. [80]) shows striking similarity to our results. Therefore, our method grasps reasonably well the stationary state. However, there is much more to Brazil nut effect, for example conduction eddies [79], friction and arching [80], that our approach cannot explain.

The most realistic case we studied in this paper was the mixture of small and big particles in an axially symmetric pore with periodically variable diameter. The variation of the diameter follows a sawtooth pattern. Therefore, the axial section of the pore resembles the two-dimensional tooth geometry investigated earlier. Numerical solution of the transport equations provided concentration dependence of the current of small and big particles, which is qualitatively very similar to both the two-dimensional tooth channel geometry and the one-dimensional pocket geometry. Also the spatial distribution of the small and big particles in the axial

section of the pore is very similar to what is observed in the two-dimensional system.

This observation provides an a posteriori justification of the generalized ASEP model in pocket geometry, which we introduced in Ref. [43]. Most importantly, the full three-dimensional solution exhibits qualitatively the same behavior of the ratchet current. This implies that such a setup can be indeed used for separation of dense mixtures of colloid particles according to their size. Quantitatively, however, the ratchet current in realistic three-dimensional geometry is smaller than in a model one-dimensional setup, because the wider sections of the pore, which play the role of pockets seen in one-dimensional model, cannot be made arbitrarily voluminous, while in one-dimensional case we are not limited in increasing the depth of the pockets. This implies that we actually could model the three-dimensional case by one-dimensional pocket geometry, but with the provision that the depth of the pocket must be appropriately calibrated and we should expect that the pockets are relatively shallow.

Finally, let us briefly mention a direction for future research. It is natural, instead of periodically driven Brownian particles, to consider active particles which possess internal drive and change direction stochastically [81,82]. They were already widely studied in complex geometries [5] and especially the ratchet effect was explored [83–87], following the experiments with rectification of bacterial movement (see, e.g., Ref. [88]). It would be interesting to use the methods developed in our work to dense ensembles of active particles. We leave this question for future work.

ACKNOWLEDGMENT

We thank K. Netočný for inspiring discussions and for providing us with his unpublished results.

-
- [1] S. Matthias and F. Müller, *Nature (London)* **424**, 53 (2003).
 - [2] P. Hänggi and F. Marchesoni, *Rev. Mod. Phys.* **81**, 387 (2009).
 - [3] D. Di Carlo, J. F. Edd, K. J. Humphry, H. A. Stone, and M. Toner, *Phys. Rev. Lett.* **102**, 094503 (2009).
 - [4] P. S. Burada, P. Hänggi, F. Marchesoni, G. Schmid, and P. Talkner, *ChemPhysChem* **10**, 45 (2009).
 - [5] C. Bechinger, R. Di Leonardo, H. Löwen, C. Reichhardt, G. Volpe, and G. Volpe, *Rev. Mod. Phys.* **88**, 045006 (2016).
 - [6] G. Segré and A. Silberberg, *J. Fluid Mech.* **14**, 136 (1962).
 - [7] L. R. Huang, E. C. Cox, R. H. Austin, and J. C. Sturm, *Science* **304**, 987 (2004).
 - [8] C. Kettner, P. Reimann, P. Hänggi, and F. Müller, *Phys. Rev. E* **61**, 312 (2000).
 - [9] C. Marquet, A. Buguin, L. Talini, and P. Silberzan, *Phys. Rev. Lett.* **88**, 168301 (2002).
 - [10] D. Reguera, G. Schmid, P. S. Burada, J. M. Rubí, P. Reimann, and P. Hänggi, *Phys. Rev. Lett.* **96**, 130603 (2006).
 - [11] D. Reguera, A. Luque, P. S. Burada, G. Schmid, J. M. Rubí, and P. Hänggi, *Phys. Rev. Lett.* **108**, 020604 (2012).
 - [12] X. Yang, C. Liu, Y. Li, F. Marchesoni, P. Hänggi, and H. P. Zhang, *Proc. Natl. Acad. Sci. USA* **114**, 9564 (2017).
 - [13] F. Slanina, *Phys. Rev. E* **99**, 012604 (2019).
 - [14] F. Slanina and P. Kalinay, *Phys. Rev. E* **100**, 032606 (2019).
 - [15] F. Slanina, *Phys. Rev. E* **102**, 052601 (2020).
 - [16] K. Mathwig, F. Müller, and U. Gösele, *New J. Phys.* **13**, 033038 (2011).
 - [17] Q.-H. Wei, C. Bechinger, and P. Leiderer, *Science* **287**, 625 (2000).
 - [18] A. J. Liu, S. R. Nagel, W. van Saarloos, and M. Wyart, in: *Dynamical Heterogeneities in Glasses, Colloids, and Granular Media*, edited by L. Berthier, G. Biroli, J.-P. Bouchaud, L. Cipelletti, and W. van Saarloos (Oxford University Press, Oxford, UK, 2011).
 - [19] P. Charbonneau, E. I. Corwin, G. Parisi, and F. Zamponi, *Phys. Rev. Lett.* **109**, 205501 (2012).
 - [20] H. M. Jaeger, S. R. Nagel, and R. P. Behringer, *Rev. Mod. Phys.* **68**, 1259 (1996).
 - [21] T. Aste and D. Weaire, *The Pursuit of Perfect Packing* (Taylor and Francis, Boca Raton, FL, 2008).
 - [22] S. Torquato and F. H. Stillinger, *Rev. Mod. Phys.* **82**, 2633 (2010).
 - [23] G. Parisi and F. Zamponi, *Rev. Mod. Phys.* **82**, 789 (2010).

- [24] B. Derrida, *Phys. Rep.* **301**, 65 (1998).
- [25] T. Kriecherbauer and J. Krug, *J. Phys. A: Math. Theor.* **43**, 403001 (2010).
- [26] L.-H. Gwa and H. Spohn, *Phys. Rev. A* **46**, 844 (1992).
- [27] B. Derrida, E. Domany, and D. Mukamel, *J. Stat. Phys.* **69**, 667 (1992).
- [28] G. Schütz, *Phys. Rev. E* **47**, 4265 (1993).
- [29] B. Derrida, M. R. Evans, V. Hakim, and V. Pasquier, *J. Phys. A: Math. Gen.* **26**, 1493 (1993).
- [30] B. Derrida, S. A. Janowsky, J. L. Lebowitz, and E. R. Speer, *J. Stat. Phys.* **73**, 813 (1993).
- [31] S. Sandow, *Phys. Rev. E* **50**, 2660 (1994).
- [32] B. Schmittmann and R. K. P. Zia, *Statistical Mechanics of Driven Diffusive System, Phase Transitions and Critical Phenomena*, edited by C. Domb and J. Lebowitz (Elsevier, Amsterdam, 1995), Vol. 17.
- [33] G. M. Schütz, *J. Stat. Phys.* **88**, 427 (1997).
- [34] G. M. Schütz, *Exactly Solvable Models for Many-body Systems Far from Equilibrium*, Phase Transitions and Critical Phenomena, edited by C. Domb and J. Lebowitz (Elsevier, Amsterdam, 2001), Vol. 19.
- [35] R. A. Blythe and M. R. Evans, *J. Phys. A: Math. Theor.* **40**, R333 (2007).
- [36] A. Gabel, P. L. Krapivsky, and S. Redner, *Phys. Rev. Lett.* **105**, 210603 (2010).
- [37] U. Basu and P. K. Mohanty, *Phys. Rev. E* **79**, 041143 (2009).
- [38] U. Basu and P. K. Mohanty, *Phys. Rev. E* **82**, 041117 (2010).
- [39] U. Basu and P. K. Mohanty, *J. Stat. Mech.* (2010) L03006.
- [40] Priyanka, A. Ayyer, and K. Jain, *Phys. Rev. E* **90**, 062104 (2014).
- [41] I. Pinkoviezky and N. S. Gov, *New J. Phys.* **15**, 025009 (2013).
- [42] P. L. Krapivsky, *J. Stat. Mech.: Theor. Exp.* (2013) P06012.
- [43] Y. A. Humenyuk, M. Kotrla, K. Netočný, and F. Slanina, *Phys. Rev. E* **101**, 032608 (2020).
- [44] Y. A. Humenyuk, M. Kotrla, and F. Slanina, *J. Stat. Mech.: Theor. Exp.* (2021) 033209.
- [45] F. Slanina, M. Kotrla, and K. Netočný, *Phys. Rev. E* **106**, 014610 (2022).
- [46] C. Kipnis, C. Landim, and S. Olla, *Commun. Pure Appl. Math.* **47**, 1475 (1994).
- [47] T. Seppäläinen, *Ann. Probab.* **27**, 361 (1999).
- [48] C. Kipnis and C. Landim, *Scaling Limits of Interacting Particle Systems* (Springer-Verlag, Berlin, 1999).
- [49] T. Becker, K. Nelissen, B. Cleuren, B. Partoens, and C. Van den Broeck, *Phys. Rev. Lett.* **111**, 110601 (2013).
- [50] T. Becker, K. Nelissen, B. Cleuren, B. Partoens, and C. Van den Broeck, *Phys. Rev. E* **90**, 052139 (2014).
- [51] C. Arita, P. L. Krapivsky, and K. Mallick, *Phys. Rev. E* **90**, 052108 (2014).
- [52] C. Arita, P. L. Krapivsky, and K. Mallick, *Phys. Rev. E* **95**, 032121 (2017).
- [53] H. Spohn, *Large Scale Dynamics of Interacting Particles* (Springer-Verlag, Berlin, 1991).
- [54] A. M. S. Tremblay, M. Arai, and E. D. Siggia, *Phys. Rev. A* **23**, 1451 (1981).
- [55] H. Spohn, *J. Stat. Phys.* **154**, 1191 (2014).
- [56] H. Spohn and G. Stoltz, *J. Stat. Phys.* **160**, 861 (2015).
- [57] V. Popkov, J. Schmidt, and G. M. Schütz, *Phys. Rev. Lett.* **112**, 200602 (2014).
- [58] V. Popkov, A. Schadschneider, J. Schmidt, and G. M. Schütz, *Proc. Natl. Acad. Sci. USA* **112**, 12645 (2015).
- [59] V. Popkov, A. Schadschneider, J. Schmidt, and G. M. Schütz, *J. Stat. Mech.: Theor. Exp.* (2016) 093211.
- [60] Z. Chen, J. de Gier, I. Hiki, and T. Sasamoto, *Phys. Rev. Lett.* **120**, 240601 (2018).
- [61] L. Bertini, A. De Sole, D. Gabrielli, G. Jona-Lasinio, and C. Landim, *J. Stat. Phys.* **107**, 635 (2002).
- [62] L. Bertini, A. De Sole, D. Gabrielli, G. Jona-Lasinio, and C. Landim, *Rev. Mod. Phys.* **87**, 593 (2015).
- [63] C. Arita, P. L. Krapivsky, and K. Mallick, *J. Phys. A: Math. Theor.* **51**, 125002 (2018).
- [64] M. Bruna and S. J. Chapman, *J. Chem. Phys.* **137**, 204116 (2012).
- [65] E. Teomy and Y. Shokef, *Phys. Rev. E* **95**, 022124 (2017).
- [66] M. Sellitto, *Phys. Rev. E* **102**, 050101(R) (2020).
- [67] C. Cattuto, R. Brito, U. Marini, Bettolo Marconi, F. Nori, and R. Soto, *Phys. Rev. Lett.* **96**, 178001 (2006).
- [68] T. R. Kirkpatrick, J. M. Ortiz de Zárate, and J. V. Sengers, *Phys. Rev. Lett.* **110**, 235902 (2013).
- [69] A. Aminov, Y. Kafri, and M. Kardar, *Phys. Rev. Lett.* **114**, 230602 (2015).
- [70] M. Sellitto, *J. Phys. A: Math. Theor.* **53**, 01LT01 (2020).
- [71] K. Netočný and F. Slanina (unpublished).
- [72] I. Derényi and T. Vicsek, *Phys. Rev. Lett.* **75**, 374 (1995).
- [73] F. Slanina, *Phys. Rev. E* **80**, 061135 (2009).
- [74] A. Rosato, K. J. Strandburg, F. Prinz, and R. H. Swendsen, *Phys. Rev. Lett.* **58**, 1038 (1987).
- [75] G. M. Whitesides, *Nature (London)* **442**, 368 (2006).
- [76] K. Ahmad and I. J. Smalley, *Powder Technol.* **8**, 69 (1973).
- [77] D. A. Huerta and J. C. Ruiz-Suárez, *Phys. Rev. Lett.* **92**, 114301 (2004).
- [78] M. Schröter, S. Ulrich, J. Kreft, J. B. Swift, and H. L. Swinney, *Phys. Rev. E* **74**, 011307 (2006).
- [79] T. Pöschel and H. J. Herrmann, *Europhys. Lett.* **29**, 123 (1995).
- [80] A. Saez, F. Vivanco, and F. Melo, *Phys. Rev. E* **72**, 021307 (2005).
- [81] P. Romanczuk, M. Bär, W. Ebeling, B. Lindner, and L. Schimansky-Geier, *Eur. Phys. J. Spec. Top.* **202**, 1 (2012).
- [82] E. Fodor and M. C. Marchetti, *Physica A* **504**, 106 (2018).
- [83] L. Angelani, A. Costanzo, and R. Di Leonardo, *Europhys. Lett.* **96**, 68002 (2011).
- [84] P. K. Ghosh, V. R. Misko, F. Marchesoni, and F. Nori, *Phys. Rev. Lett.* **110**, 268301 (2013).
- [85] B.-Q. Ai, Q.-Y. Chen, Y.-F. He, F.-G. Li, and W.-R. Zhong, *Phys. Rev. E* **88**, 062129 (2013).
- [86] X. Ao, P. K. Ghosh, Y. Li, G. Schmid, P. Hänggi, and F. Marchesoni, *Eur. Phys. J. Spec. Top.* **223**, 3227 (2014).
- [87] C. J. Olson Reichhardt and C. Reichhardt, *Annu. Rev. Condens. Matter Phys.* **8**, 51 (2017).
- [88] G. Mahmud, C. J. Campbell, K. J. M. Bishop, Y. A. Komarova, O. Chaga, S. Soh, S. Huda, K. Kandere-Grzybowska, and B. A. Grzybowski, *Nat. Phys.* **5**, 606 (2009).